NANO LETTERS

Letter

pubs.acs.org/NanoLett

In Situ Nanomechanical Measurements of Interfacial Strength in Membrane-Embedded Chemically Functionalized Si Microwires for Flexible Solar Cells

Clara J. Cho,[†,⊥] Leslie O'Leary,[‡,⊥] Nathan S. Lewis,[‡,§,∥] and Julia R. Greer*[,†,§]

[†]Division of Engineering and Applied Sciences, [‡]Division of Chemistry and Chemical Engineering, [§]The Kavli Nanoscience Institute at Caltech, and [∥]The Beckman Institute at Caltech, California Institute of Technology, Pasadena, California 91125, United States

Supporting Information

ABSTRACT: Arrays of vertically aligned Si microwires embedded in polydimethylsiloxane (PDMS) have emerged as a promising candidate for use in solar energy conversion devices. Such structures are lightweight and concurrently demonstrate competitive efficiency and mechanical flexibility. To ensure reliable functioning under bending and flexing, strong interfacial adhesion between the nanowire and the matrix is needed. In situ uniaxial tensile tests of individual, chemically functionalized, Si microwires embedded in a compliant PDMS matrix reveal that chemical functionality on Si microwire surfaces is directly correlated with interfacial adhesion strength. Chemical functionalization can therefore serve as an effective methodology for accessing a wide range of interfacial adhesion between the rigid constituents and the soft polymer matrix; the adhesion can be quantified by measuring the mechanical strength of such systems.

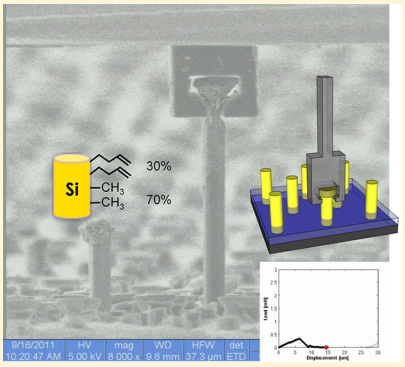

KEYWORDS: *Si microwires, fiber pull-out, in situ tension, flexible solar cells mechanical properties*

Light-weight and flexible device platforms are of interest for a wide range of applications, specifically those in which incorporation of high-performing electronic structures into inexpensive, stretchable packaging material can lower the materials cost and facilitate scalable manufacturing processes.[1−3] Extensive studies have been performed on the structural integrity of micro- and nanostructures integrated into flexible and stretchable substrates, with example applications in chemical sensors,[4] artificial skin technology,[5,6] and liquid crystal displays.[7] Vertically aligned micro- and nanostructures have been integrated into flexible and/or stretchable substrates, with potential technological applications ranging from photovoltaics[8−13] and light-emitting diodes[14−16] to chemical sensors[17] and energy harvesting devices.[18] The mechanical characterization of vertically aligned, regularly spaced rigid constituents embedded into a soft, flexible thin-film matrix has received relatively little attention. Importantly, such systems are distinct in several key aspects from well-characterized fiber-reinforced composites. First, lithographically patterned catalysts enable precise control over the vertical arrangements of nano- and microwires facilitating the ordering from quasi-random to periodic,[12] thus making such structures well suited to explore the mechanical response as a function of different wire periodicity. Second, all of the rigid constituents are arranged on a single level, rather than being randomly spread within the matrix, as is the case in the more traditional composites (for example, carbon-fiber reinforced resins), in which little control exists over fiber orientation, spacing, and continuity. Finally, the wires are embedded along the shortest length of the matrix, perpendicular to both the film surface and the underlying substrate. Therefore, understanding the mechanical properties of these unique, mechanically untapped composite systems, on both the array and individual constituent levels, is needed to facilitate their reliable insertion into flexible device platforms.

Vertically aligned, radial p−n junction Si microwire arrays embedded in a polydimethylsiloxane (PDMS) matrix have demonstrated the potential for high solar energy conversion efficiencies by taking advantage of the combined short radial minority carrier diffusion length and long optical absorption depth.[8−13] In these solar cells, the vertically aligned Si nanowires are positioned periodically within the polymer matrix, and mechanical flexibility is enabled via bending and stretching along the transverse direction of the composite. To ensure the reliable functioning under bending and flexing, strong interfacial adhesion between the nanowire and the matrix is needed. These interfaces serve as the medium for elastic stress transfer and therefore are likely sources of in-use damage initiation.[19] Several methods have been utilized to improve fiber−polymer bonding in composites, for example, the addition of adhesion promoters to the resin, tuning the surface roughness, and modification of the chemical interactions at the fiber−polymer interface.[20] In all of these studies the fiber diameters are generally on the order of 10^{-2}−10^{-1}m, complicating the investigation of the effects of particular

Received: April 14, 2012
Revised: May 9, 2012
Published: May 21, 2012

chemical bonds on such large systems. The mechanical properties of traditional composites are also generally assessed at the full-composite scale, as opposed to via individual fiber pull-out tests, although the latter are becoming more commonplace. The micrometer-sized Si microwire–PDMS composites allow for elucidation of the specific details of how chemical intermolecular bonding contributes to, or detracts from, the interfacial adhesion strength.

We report herein *in situ* nanomechanical measurements of the interfacial shear strengths of individual Si wires that have been functionalized with a variety of chemical functionality and embedded into a PDMS matrix. Individual wire pull-out tests have been conducted on single crystalline Si microwires that had different interfacial bonding mechanisms to the PDMS matrix using a custom-made *in situ* nanomechanical instrument, SEMentor. The interfacial shear strength was then calculated based on the maximum applied load at the instance of debonding. We note that these experiments were not carried out on the voltage producing junctions—either with functionalized or H-terminated surfaces. This does not detract from their potential use in solar cell arrays because it has been reported that the chemical functionalization improved the properties in some photoelectrochemical and Schottky junction devices due to the kinetic stability imparted by the Si–C bonds.[21−23]

Chemical Functionalization. Figure 1 depicts the processing steps used to form the Si–PDMS matrix composites. PDMS is an elastomeric material that cures via hydrosilylation cross-linking polymerization. The hydrosilylation reaction involves the addition of silicon–hydride (Si–H) across a carbon–carbon double bond (C=C) in the presence of a metal catalyst (i.e., Pt) or ultraviolet (UV) light to form silicon–carbon (Si–C) bonds. This reaction can also occur between the chemically modified Si surfaces and the corresponding end group present in the prepolymer mix, providing an approach to engineer a strong interface by covalent attachment of Si surface to the PDMS matrix.[24,25] In the absence of deliberate surface modification, the faceted Si microwire surfaces form a thin layer of native oxide upon exposure to air, so the wires interact with the cured PDMS matrix via intermolecular forces, including H-bonding and van der Waals interactions between SiO_2 and the solidified PDMS silanol backbone.[26,27] To facilitate covalent bonding, two sets of Si wires were chemically modified, resulting in (1) H-terminated and (2) mixed butenyl-/CH_3-terminated surfaces (see inset in Figure 3 and Figure 4c). Surfaces were functionalized with a combination of butenyl and CH_3 termination because due to steric hindrance the fully butenyl-terminated surface has a limited ability to react with the prepolymer mix.[24] Chemical modification of the wire surfaces was performed prior to spin casting the PDMS prepolymer mix into the wire array. Two additional sets of Si wires were prepared with (3) methyl- and (4) octadecyl-terminated surfaces, to ascertain the effects of nonbonding van der Waals interactions as well as the dependence of the interaction on the alkyl-chain length.

Mechanical Characterization. Individual wire pull-out tests, similar to single fiber pull-out tests that are often performed in fiber-reinforced composites, were performed to measure the interfacial strength between the Si microwires and the PDMS matrix in Si–PDMS composites.[28−30] Individual wire pullout tests were performed in a custom-built in situ mechanical deformation instrument, SEMentor, comprised of

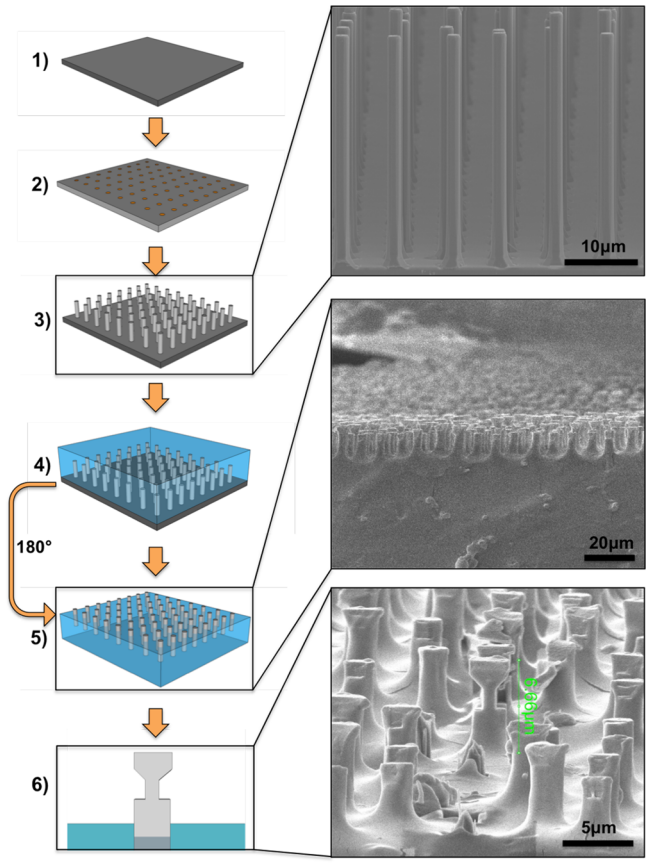

Figure 1. Left: Schematic representation of the fabrication steps for Si–PDMS composite matrix. Step 1: Thermal oxide was grown on Si (111) wafer with low miscut angle (±0.1°). Step 2: Cu catalyst was deposited into patterned holes through the oxide. Step 3: 25–35 μm tall Si wires were grown via VLS growth process to height. Step 4: PDMS (Sylgard 184) solution was spin cast onto the Si wire arrays and thermally cured. Step 5: The Si–PDMS matrix was peeled from the Si wafer and flipped upside down. Step 6: The exposed end of a wire was milled out into a T-shaped handle via FIB in preparation to be tensed using a diamond microgrip. Right: SEM images corresponding to fabrication steps 3, 5, and 6.

scanning electron microscope (SEM) and a nanomechanical module similar to a nanoindenter.[31] To prepare Si wires embedded in PDMS for such tensile testing, focused ion beam (FIB) was used to shape the exposed wire tips into a "dog-bone" configuration. During the experiment, the sample stage was manually controlled to position the "dog-bone" shaped tip inside of the FIB-machined diamond tension grips. Tensile experiments were carried out at a constant nominal displacement rate of 50 nm/s, and each wire was lifted by 30 μm away from the surface. Most of the wires completely debonded from the matrix before reaching the final displacement limit. On each sample set, 5–6 independent measurements were obtained.

Results. Figure 2 displays representative time-lapse SEM video frames with concurrent load vs normalized displacement data that were generated by SEMentor during a typical pullout test (full movies are provided in Supporting Information). Three distinct regions are evident in the plot. Region 1 corresponds to the initial elastic tensile loading of the composite with a fully bonded interface, as revealed by the corresponding SEM image. Wire debonding occurred at the onset of region 2, at a maximum load of 0.33 mN, followed by a marked (~3×) load drop over a short, 1–2 μm, displacement.

dx.doi.org/10.1021/nl3014007 | *Nano Lett.* 2012, 12, 3296–3301

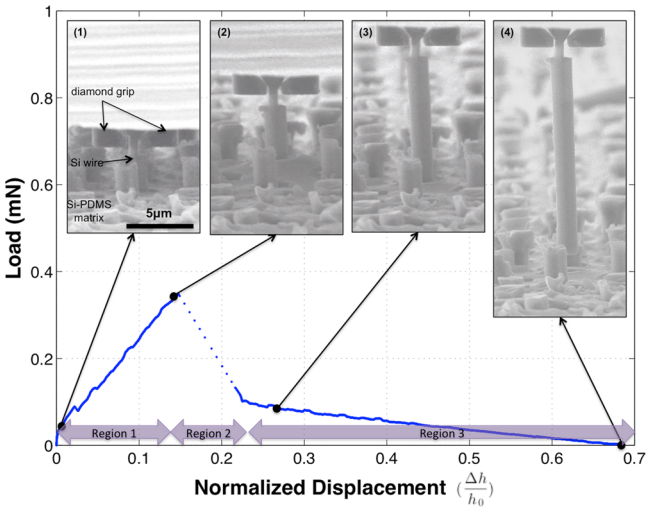

Figure 2. Representative load vs displacement behavior of a Si microwire being pulled out from a PDMS matrix. The displacement is normalized by the wire height. SEM images correspond to three distinct regions: (1) elastic loading of the Si–PDMS matrix, (2) interfacial debonding with partial removal of the wire from the PDMS matrix, and (3) frictional stress between the debonded wire and the PDMS matrix. (4) An image of the completely removed wire with residual PDMS, indicating that failure was at least not entirely at the PDMS–wire interface.

During this load drop, the prescribed displacement rate of 50 nm/s was difficult to maintain, because the nanoindenter is inherently a load-controlled instrument, and the feedback loop requires time to adjust the displacement rate accurately. Consequently, the displacement rate during this debonding event was higher than prescribed, typically restoring to the prescribed value in 2–3 s. Region 3 corresponds to dragging of the debonded wire out of the matrix in a process dominated by frictional sliding at the interface, during which the applied force gradually decreased as more of the wire was released from the matrix. In this region, the matrix around the wire did not visibly deform, and most of the stored elastic energy was therefore presumably absorbed by friction. The underlying physical deformation mechanism after initial debonding varied depending on the type of surface functionalization. Broken chemical bonds were irreparable in bonding induced interactions, whereas in hydrogen and nonbonding cases, the adjacent molecules reconfigured themselves so as to keep the interface partially intact during frictional sliding.[32]

Figure 3 depicts representative pull-out data for the four types of functionalized Si wires, with the average interfacial shear stress (τ) plotted against raw displacement normalized by the total wire length. For clarity, each data set has been vertically offset by unity. The interfacial shear stress was calculated by dividing the applied axial load (F) by the interfacial contact area between the wire and PDMS: $\tau = (F/(2\pi rL))$, where r and L are radius and length of the wire, respectively. The overall average interfacial shear strength, τ_{max}, was estimated by dividing the maximum applied axial load, F_{max}, at the instance of debonding by the entire surface area of the wire: $\tau_{max} = F_{max}/(2\pi rL)$. Such a calculation assumes that the Si wire carries all of the axial load in tension, and hence the matrix only carries shear stress, as described in detail in the shear lag model (see Supporting Information).[33]

Table 1 shows the interfacial shear strengths for each sample type, along with the average normalized displacement at the instance of debonding, to characterize and compare the extent of deformation prior to microwire detachment. The H-terminated Si microwire surface exhibited the highest interfacial shear strength (8 MPa), followed by the methyl-terminated surface (4.1 MPa), the mixed butenyl-/methyl-terminated surface (3.5 MPa), with the octadecyl-terminated surface having the lowest interfacial shear strength (1.5 MPa) of all the samples studied. SEM images of completely pulled out wires from each sample group, shown next to their respective stress–strain curves in Figure 3, revealed that samples with lower interfacial strengths retained their faceted, pristine surfaces, while those with higher interfacial strengths possessed residual PDMS, presumably as a result of incomplete debonding during tensile loading. The adhered PDMS is also indicative of matrix cracking, implying that the work of fracture includes a significant amount of plastic dissipation, which can be estimated by calculating the work of adhesion at the wire–polymer interface (see Supporting Information).

Discussion. Figure 4a shows the mean interfacial shear strengths of each functional group vs the predicted bond strength. A positive correlation was clearly evident for H-, methyl-, and octadecyl-terminated Si wire surfaces.

The mixed butenyl-/methyl-terminated Si surfaces exhibited slightly lower interfacial shear strengths than the methyl-terminated Si surfaces. This behavior is consistent with the limited availability of the methylhydrogen siloxane oligomers in the PDMS prepolymer mix to react with the butenyl-terminated surface, since such systems contain 10 parts of vinyl-terminated dimethyl siloxane oligomers and only 1 part of methylhydrogen siloxane oligomers. Thus, the butenyl-terminated sites can not react with the matrix but instead serve as the slightly longer carbon chains than methyl groups interacting with the PDMS primarily via nonbonding interaction. Further, the relatively long butenyl chains could displace the curing PDMS from nonfunctionalized Si sites thereby preventing covalent bonding with the desired Si–H sites.

A similar trend was observed in the normalized displacement at the instance of debonding as a function of predicted bond strength (Figure 4b). Stronger interfaces showed greater strains-at-failure, with the covalently bonded interface (H-terminated) having normalized displacement of 0.57 before onset of debonding, while the failure of the fully nonbonded samples, i.e. octadecyl-terminated Si surfaces, occurred at a normalized displacement of 0.14. Notably, the octadecyl-terminated Si surfaces had a 62% weaker shear strength than the methyl-terminated surfaces. This suggests that the adhesion mechanism was not dominated by the entanglement of polymer chains, because that would result in an increased interfacial shear strength as the alkyl-chain length increased.[32] Chemical interactions, therefore, appear to be is the dominant mechanism for adhesion in this system. The octadecyl-terminated Si thus showed lower interfacial shear strengths presumably because the Si surface was densely covered with long, nonpolar alkyl-chains, thereby preventing the PDMS from interacting with the Si surface. In contrast, the methyl-terminated Si surface had a layer of short monomer chain covering the surface and therefore is less effective at shielding Si atoms from interacting with the PDMS. This expectation was further substantiated by X-ray Photoelectron Spectroscopy (XPS) analysis of the methyl-terminated Si (110) surface, which revealed that only 71 ± 2% of the surface was chemically functionalized (Supporting Information and Table 1).

Fracture Analysis. The work of fracture was calculated based on the load vs raw displacement data, by utilizing the shear lag model for short wires embedded inside a matrix, in conjunction

dx.doi.org/10.1021/nl3014007 | *Nano Lett.* 2012, 12, 3296–3301

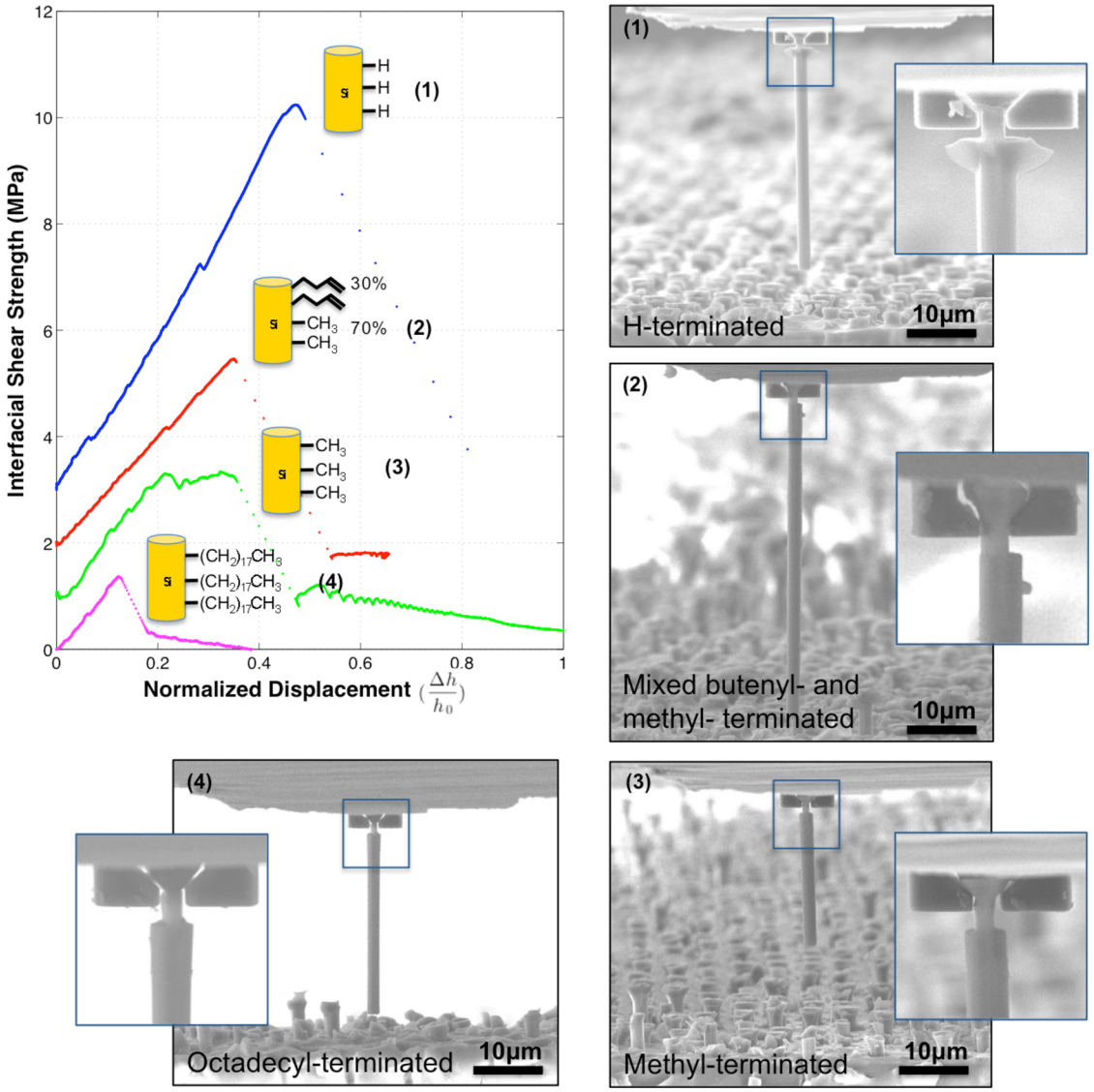

Figure 3. Interfacial shear strength vs normalized axial displacement of Si wires that had various surface functionalizations, illustrated next to each data set. Also shown are SEM images of completely removed wires for each functionalization type. The magnified SEM images (inset) correspond to the marked region, showing the PDMS residue on the wire surface.

Table 1. Interfacial Shear Strengths for Each Sample Type[a]

Surface Functionality	$\Gamma_{C\text{-}Si}$ (cm^{-2})	$\theta_{C\text{-}Si}$	Adhesion Interaction[a]	Interfacial shear strength (MPa)	Normalized displacement at debonding	Work at fracture ($J\ m^{-2}$)
H-Si(111)	-	1[b]	Covalent bond	8	0.57	124
Mixed butenyl/ CH_3-Si(011)	$5.0 \pm 0.2 \times 10^{14}$	0.52 ± 0.02[c]	Covalent bond	3.5	0.36	22
CH_3-Si(011)	$6.8 \pm 0.2 \times 10^{14}$	0.71 ± 0.02[c]	vdW interaction	4.1	0.42	33
Octadecyl-Si(011)	$2.7 \pm 0.3 \times 10^{14}$	0.28 ± 0.03[c]	vdW interaction	1.5	0.14	5

[a]Shinohara, M; kuwano, T.; Akama, I.; Kimura, Y.; Niwano, M. *J. Vac. Sci. Technol., A* **2003**, *21*(1), 25; Eremtchenko, M.; Tautz, F.S.; Ottking, R.; Polyakov, V. M.; Schwierz, F.; Cherkashinin, G.; Schaefer, J. A. *Surf. Sci.* **2005**, *582*(1), 159. [b]Predicted adhesion interaction. [c]Reconstruction with mono,di,trihydrides{1,2}. [d]$\theta_{C-Si} = \Gamma_{C-Si}/\Gamma_{Si(011)}$; as determined by XPS. Average ± standared deviation.

with performing an energy balance of the composite system, with the aim of expressing the interfacial shear stress at the instance of debonding.[29,30] The shear lag model developed by Cox primarily describes the load transfer between the fiber and a soft matrix, because it assumes that the fiber carries all of the axial load in tension, and hence the matrix only carries shear stress.[33] Because the chemically functionalized surfaces contained only a very thin, atomic-level interface, it is

dx.doi.org/10.1021/nl3014007 | *Nano Lett.* 2012, 12, 3296−3301

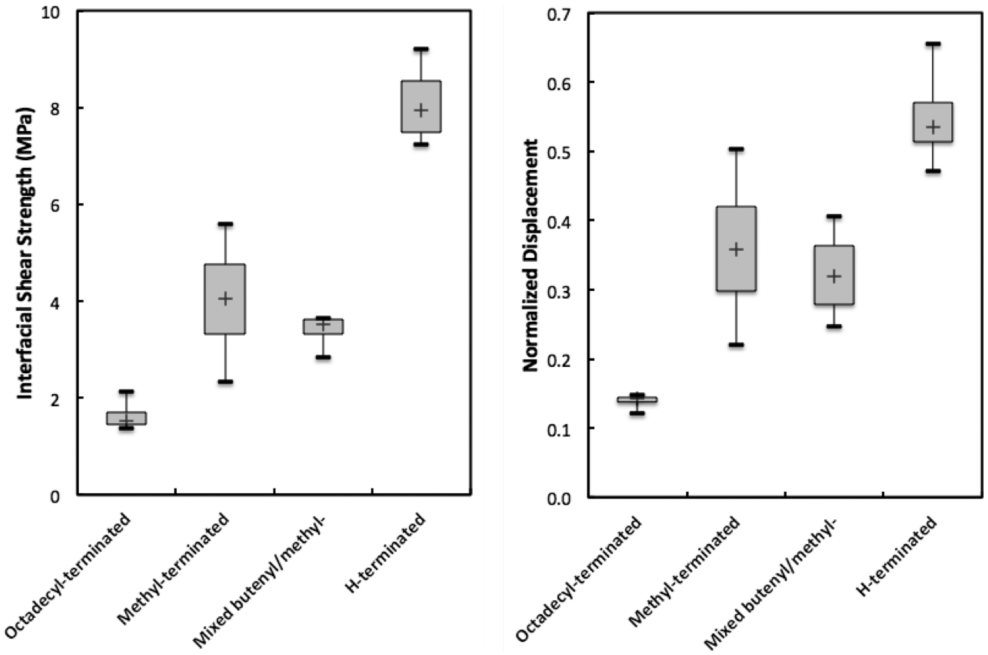

Figure 4. (a) Boxplot of interfacial shear strength vs surface functionalization, showing a positive correlation between the interfacial strength and the interaction strength. (b) Boxplot of normalized displacement at debonding vs surface chemical functionalization, also showing a positive correlation between the displacement and the interaction strength.

reasonable to not treat this system as consisting of a "three-phase" system with an interphase, as is commonly done for traditional composites.

Debonding occurs when the rate of the elastic energy released by the composite (dU_c/dL) is equal to the rate of surface energy increased due to debonding (dU_s/dL), plus the rate of elastic energy stored in the debonded wire (dU_{db}/dL):

$$\frac{dU_c}{dL} = \frac{dU_s}{dL} + \frac{dU_{db}}{dL} \quad (1)$$

By substituting the expression for the interfacial shear stress obtained from the shear lag model, the relationship between the work of fracture and interfacial shear stress is

$$G_i = \frac{\tau_i^2 r}{n^2 E_f} \quad (2)$$

where τ_i is the interfacial shear stress at debonding, E_f is the elastic modulus of the Si microwire (analogous to fiber), r is the microwire radius, and n is the dimensionless quantity defined as

$$n^2 = \frac{E_m}{E_f(1+\nu_m)\ln(R/r)}$$

Details of this derivation are provided in Supporting Information.

Table 1 lists different wire surface functionalizations, along with the average interfacial shear strengths, the work of fracture in J/m^2, and the displacement at debonding normalized by the wire length. Consistent with having the maximum interfacial shear strength relative to the other functionalized samples, H-terminated Si microwires also had the highest work of fracture, 124 J/m^2. Based on the predicted bond energy (around 1−5 J/m^2), correlated with the work of adhesion, H-terminated Si is expected to have significant plastic dissipation, which is consistent with the SEM image revealing substantial PDMS residue remaining on the wire after pull-out. The degree of such nonideal debonding, i.e., resulting in some residual PDMS attached to the wire post pull-out, is indicative of cracking in the PDMS, as is clearly demonstrated by the observation that samples with a much lower contribution of plastic dissipation to the work of fracture term, had little or no residual PDMS attached to the wire.

The interfacial shear stress was also unambiguously correlated to the interfacial bond strength, as revealed by estimating the bond energy based on the relative surface coverage obtained by XPS analysis. The facets of ⟨111⟩-oriented Si wires were represented via Wulff construction, which resulted in a hexagonal cross-section with (110) facets.[34,35] The same type of surface functionalized (110) Si as was used for XPS analysis was then utilized to estimate the coverage of these facets. The details of the XPS analysis work are provided in Supporting Information, with the ligand coverage, θ_{C-Si}, listed in Table 1. The experimentally obtained work of fracture (G_i) was anti-correlated with the relative surface coverage of the ligand (θ_{C-Si}). Using the surface coverage of functionalized groups on the surface of (110) Si side facets and the radius of gyration of individual polymer chains, the total number of bonds formed at the interface was estimated for the chemical functionalization types studied in this work (Table 1). The data also provide a path to quantify bond energy calculations, which will be described separately.

Conclusions. In situ uniaxial tensile tests of individual Si microwires embedded in a compliant PDMS matrix have revealed that the chemical functionality on Si microwire surfaces is directly correlated with the interfacial adhesion strength. Four different functionalities spanned a range of bond energies, surface coverages, and alkyl chains, respectively, were attached directly onto the Si side faces, with PDMS directly polymerizing in the presence of these functional groups. Covalent surface−matrix interactions, as were obtained with H-terminated Si, exhibited the highest interfacial shear strengths (8 MPa), followed by mixed butenyl-/methyl-terminated and methyl-terminated Si systems that formed predominantly van der

dx.doi.org/10.1021/nl3014007 | Nano Lett. 2012, 12, 3296−3301

Waals interactions (3−4 MPa) and then octadecyl-terminated Si that formed van der Waals interactions with greater separation (1−2 MPa). Chemical functionalization can therefore serve as an effective methodology for elicitation of a wide range of interfacial adhesion between the rigid constituents and the soft polymer matrix; the adhesion can be quantified by measuring the mechanical strength of such systems.

■ ASSOCIATED CONTENT

Supporting Information

Material contains sample fabrication and chemical functionalization details, interfacial shear strength, and work of fracture calculations. This material is available free of charge via the Internet at http://pubs.acs.org.

■ AUTHOR INFORMATION

Corresponding Author

*E-mail: jrgreer@caltech.edu

Author Contributions

⊥These authors contributed equally.

Notes

The authors declare no competing financial interest.

■ ACKNOWLEDGMENTS

C.J.C. gratefully acknowledges the financial support of the Resnick Institute at Caltech through her graduate fellowship and E. Warren for help with wafer patterning. L.O'L. thanks the financial support of the Link Foundation Energy fellowship. N.S.L.'s portion of this work was supported by the National Science Foundation (NSF-CHE-0911682) and (NSF- CHE-0802907). J.R.G. is grateful to the Caltech's CI-2 Innovation Grant for supporting this work.

■ REFERENCES

(1) Rogers, J. A.; Someya, T.; Huang, Y. *Science* **2010**, *327*, 1603−7.
(2) Park, S.-I.; Ahn, J.-H.; Feng, X.; Wang, S.; Huang, Y.; Rogers, J. a. *Adv. Funct. Mater.* **2008**, *18*, 2673−2684.
(3) Gleskova, H.; Cheng, I.-chun; Wagner, S.; Sturm, J.; Suo, Z. *Solar Energy* **2006**, *80*, 687−693.
(4) McAlpine, M. C.; Ahmad, H.; Wang, D.; Heath, J. R. *Nat. Mater.* **2007**, *6*, 379−84.
(5) Someya, T.; Sekitani, T.; Iba, S.; Kato, Y.; Kawaguchi, H.; Sakurai, T. *Proc. Natl. Acad. Sci. U.S.A.* **2004**, *101*, 9966.
(6) Sun, Y.; Choi, W. M.; Jiang, H.; Huang, Y. Y.; Rogers, J. a *Nat. Nanotechnol.* **2006**, *1*, 201−7.
(7) Sheraw, C. D.; Zhou, L.; Huang, J. R.; Gundlach, D. J.; Jackson, T. N.; Kane, M. G.; Hill, I. G.; Hammond, M. S.; Campi, J.; Greening, B. K.; Francl, J.; West, J. *Appl. Phys. Lett.* **2002**, *80*, 1088.
(8) Hu, L.; Chen, G. *Nano Lett.* **2007**, *7*, 3249−52.
(9) Fan, Z.; Razavi, H.; Do, J.-won; Moriwaki, A.; Ergen, O.; Chueh, Y.-L.; Leu, P. W.; Ho, J. C.; Takahashi, T.; Reichertz, L. a; Neale, S.; Yu, K.; Wu, M.; Ager, J. W.; Javey, A. *Nat. Mater.* **2009**, *8*, 648−53.
(10) Spurgeon, J. M.; Plass, K. E.; Kayes, B. M.; Brunschwig, B. S.; Atwater, H. a.; Lewis, N. S. *Appl. Phys. Lett.* **2008**, *93*, 032112.
(11) Plass, K. E.; Filler, M. a.; Spurgeon, J. M.; Kayes, B. M.; Maldonado, S.; Brunschwig, B. S.; Atwater, H. a.; Lewis, N. S. *Adv. Mater.* **2009**, *21*, 325−328.
(12) Kelzenberg, M. D.; Boettcher, S. W.; Petykiewicz, J. a; Turner-Evans, D. B.; Putnam, M. C.; Warren, E. L.; Spurgeon, J. M.; Briggs, R. M.; Lewis, N. S.; Atwater, H. a *Nat. Mater.* **2010**, *9*, 239−44.
(13) Putnam, M. C.; Boettcher, S. W.; Kelzenberg, M. D.; Turner-Evans, D. B.; Spurgeon, J. M.; Warren, E. L.; Briggs, R. M.; Lewis, N. S.; Atwater, H. a. *Energy Environ. Sci.* **2010**, *3*, 1037.
(14) Nadarajah, A.; Word, R. C.; Meiss, J.; Könenkamp, R. *Nano Lett.* **2008**, *8*, 534−7.
(15) Lai, E.; Kim, W.; Yang, P. *Nano Res.* **2008**, *1*, 123−128.
(16) Chen, J.; Könenkamp, R. *Appl. Phys. Lett.* **2003**, *82*, 4782.
(17) Chen, J.; Wang, K.; Hartman, L.; Zhou, W. *J. Phys. Chem. C* **2008**, *112*, 16017−16021.
(18) Wang, Z. L.; Song, J. *Science (New York, N.Y.)* **2006**, *312*, 242−6.
(19) Achenbach, J.; Zhu, H. *J. Mech. Phys. Solids* **1989**, *37*, 381−393.
(20) Tang, L.; Kardos, J. L. *Polym. Compos.* **1997**, 18.
(21) Maldonado, S.; Knapp, D.; Lewis, N. S. *J. Am. Chem. Soc.* **2008**, *130*, 3300−3301.
(22) Johansson, E.; Boettcher, S. W.; Leary, L. E. O.; Poletayev, A. D.; Maldonado, S.; Brunschwig, B. S.; Lewis, N. S. *J. Phys. Chem. C* **2011**, *2*, 8594−8601.
(23) Price, M. J.; Foley, J. M.; May, R. a.; Maldonado, S. *Appl. Phys. Lett.* **2010**, *97*, 083503.
(24) O'Leary, L. E.; Johansson, E.; Brunschwig, B. S.; Lewis, N. S. *J. Phys. Chem. B* **2010**, *114*, 14298−302.
(25) Langner, A.; Panarello, A.; Rivillon, S.; Vassylyev, O.; Khinast, J. G.; Chabal, Y. J. *J. Am. Chem. Soc.* **2005**, *127*, 12798−9.
(26) Tsige, M.; Soddemann, T.; Rempe, S. B.; Grest, G. S.; Kress, J. D.; Robbins, M. O.; Sides, S. W.; Stevens, M. J.; Webb, E. *J. Chem. Phys.* **2003**, *118*, 5132.
(27) Haick, H.; Hurley, P. T.; Hochbaum, A. I.; Yang, P.; Lewis, N. S. *J. Am. Chem. Soc.* **2006**, *128*, 8990−1.
(28) Hsueh, C. *Mater. Sci. Eng., A* **1990**, *123*, 1−11.
(29) Piggott, M. *Compos. Sci. Technol.* **1991**, *42*, 57−76.
(30) Piggott, M. R. *Load Bearing Fiber Composites*; Kluwer Academic Publisher: Norwell, MA (USA), 2002.
(31) Kim, J.-Y.; Greer, J. R. *Acta Mater.* **2009**, *57*, 5245−5253.
(32) Wang, T.; Dalton, A. B.; Keddie, J. L. *Macromolecules* **2008**, *41*, 7656−7661.
(33) Cox, H. *Br. J. Appl. Phys.* **1952**, *3*, 72.
(34) Migas, D. B.; Borisenko, V. E. *J. Appl. Phys.* **2009**, *105*, 104316.
(35) Schmidt, V.; Wittemann, J. V.; Gösele, U. *Chem. Rev.* **2010**, *110*, 361−88.